ACS OMEGA

Article

Cite This: ACS Omega 2019, 4, 13309−13318

http://pubs.acs.org/journal/acsodf

Xylindein: Naturally Produced Fungal Compound for Sustainable (Opto)electronics

Gregory Giesbers,[†] Jonathan Van Schenck,[†] Alexander Quinn,[†] Ray Van Court,[‡] Sarath M. Vega Gutierrez,[‡] Seri C. Robinson,[‡] and Oksana Ostroverkhova*[,†]

[†]Department of Physics and [‡]Department of Wood Science and Engineering, Oregon State University, Corvallis, Oregon 97331, United States

Supporting Information

ABSTRACT: Organic semiconductors are of interest for (opto)electronic applications due to their low cost, solution processability, and tunable properties. Recently, natural product-derived organic pigments attracted attention due to their extraordinary environmental stability and unexpectedly good optoelectronic performance, in spite of only partially conjugated molecular structure. Fungi-derived pigments are a naturally sourced, sustainable class of materials that are largely unexplored as organic semiconductor materials. We present a study of the optical and electronic properties of a fungi-derived pigment xylindein, which is secreted by the wood-staining fungi *Chlorociboria aeruginosa*, and its blends with poly(methyl methacrylate) (PMMA) and crystalline nanocellulose (CNC). Optical absorption spectra of xylindein revealed the presence of two tautomers whose structures and properties were established using density functional theory. Pronounced pigment aggregation in polar solvents and in films, driven by intermolecular hydrogen bonding, was also observed. The pigment exhibited high photostability, electron mobility up to 0.4 $cm^2/(V\ s)$ in amorphous films, and thermally activated charge transport and photoresponse with activation energies of ∼0.3 and 0.2 eV, respectively. The dark and photocurrents in xylindein:PMMA blends were comparable to those in pristine xylindein film, whereas blends with CNC exhibited lower currents due to inhomogeneous distribution of xylindein in the CNC.

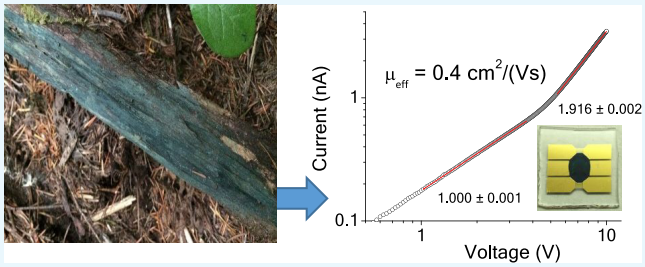

INTRODUCTION

Organic (opto)electronic materials are of interest due to their low cost and tunable properties;[1] a broad range of their applications, from photovoltaics to three-dimensional displays, have been demonstrated.[2] Solution processable materials that can be cast into thin films using various solution deposition techniques are especially advantageous.[3] One of the bottlenecks that complicates organic materials processing and device fabrication, as well as hinders commercialization, is their relatively low stability with respect to photo- and/or thermal degradation. Therefore, organic (opto)electronic materials that exhibit enhanced stability are of considerable interest.

Over the past decade, there has been a considerable research effort focusing on sustainable, natural product-derived materials for organic electronics. These include biodegradable and biocompatible substrate materials (e.g., polyester elastomers), polymer dielectric and electrodes, and plant- or animal-derived active layers.[4−6] Examples of the latter include carotenoids, porphyrins, and anthraquinone derivatives, with the most successful examples being the indigo and tyrian purple dyes,[5,7,8] which exhibited ambipolar charge transport with balanced organic field-effect transistor (OFET) carrier mobilities of 0.3−0.4 $cm^2/(V\ s)$ in crystalline films. Additionally, indigo's structural isomer, isoindigo, has been used as a building block for donor−acceptor (D/A) oligomers and co-polymers serving as donors in bulk heterojunction organic solar cells with power conversion efficiencies of up to 8.2%.[9] Another successful example is animal-derived diketopyrrolopyrrole derivative used as a building block in D/A co-polymers with OFET charge carrier mobilities of 10−12 $cm^2/(V\ s)$.[9] Moreover, some derivatives, such as quinacridone (derived from naturally occurring acridone), exhibited extraordinary photoconductive properties: an external quantum efficiency of 10% in a single-layer Schottky diode, three orders of magnitude higher than that in benchmark pentacene films in a similar device geometry.[10] Success of the derivatives of natural origin, and with unconventional molecular structure, has been referred to as an exciting paradigm shift from the traditional requirements of an organic semiconductor molecule to necessarily possess a fully π-conjugated core, instead focusing on the importance of H-bonding for photophysics and molecular packing.[11] Additionally, many of such "unconventional" derivatives exhibited an enhanced stability with respect to environmental factors,[12,13] thus addressing a major issue of performance degradation in organic electronics. An example of unconventional and highly stable molecule of potential interest

Received: May 21, 2019
Accepted: July 11, 2019
Published: August 6, 2019

DOI: 10.1021/acsomega.9b01490
ACS Omega 2019, 4, 13309−13318

for organic electronics is xylindein, which is a blue-green pigment (Figure 1) secreted by the nonpathogenic wood-

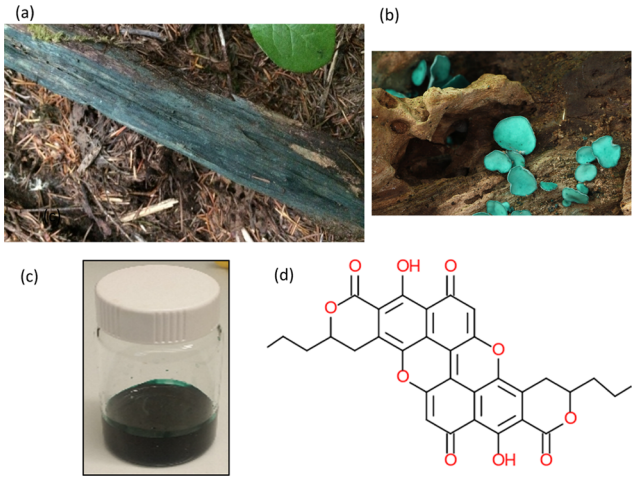

Figure 1. (a, b) *C. aeruginosa* producing blue-green pigment xylindein on the decaying wood. (c) The extracted pigment in the solution. (d) Molecular structure of xylindein.

staining fungi *Chlorociboria aeruginosa*. Many fungi produce pigments for use in resource capture/territorial defense, ultraviolet (UV) resistance, and prevention of desiccation. Only a very selected group of fungi, generally the wood soft-rotting fungi in the Ascomycetes, produce pigments that can penetrate deeply into wood.[14] These special pigments, referred to as "spalting" pigments, have antifungal properties and are secreted by fungi to defend territory (the wood matrix) while they grow into the substrate. Spalting fungi generally grow very slowly, and the distribution of the pigment into the wood allows them the time they need to colonize. Since it can take years for a given spalting fungus to colonize a log, the pigment it makes must be stable, under UV light, in water, heat, and other extreme environmental conditions. Their persistence is well documented, the blue-green pigment xylindein of Figure 1 can be found in intarsia and marquetry woodworks as far back as the 1400s, still as vibrant as samples collected today.[15,16] The two *Chlorociboria* species *C. aeruginosa* and *Chlorociboria aeruginascens*, both of which produce xylindein, have a worldwide distribution, and the wood stained by their colonization is readily available in the Pacific Northwest of the United States, among many other regions. Though pigment generation is slow in the wild, it can be significantly increased under laboratory conditions and requires only standard 2% malt agar substrates (with some added sterilized, rotted wood) for growth.[17−19] No additional heat, nutrients, or movement is required.

Recently, we specifically demonstrated that xylindein shows extraordinary stability under UV excitation and self-healing capabilities.[20] Current interest in xylindein revolves primarily around the controlled introduction of the pigment into high-value wood products for aesthetic purposes.[19,21] Here, we seek to explore xylindein as a sustainable (opto)electronic material. We also note that our toxicity studies indicate that xylindein is nontoxic (see the Supporting Information), which makes it potentially attractive for applications requiring biocompatibility.

The core structure of the xylindein molecule is a peri-xanthenoxanthene (PXX),[22−26] derivatives of which (3,9-diphenyl−PXX and 3,9-bis(*p*-propylphenyl)−PXX) were shown to exhibit hole mobilities of up to ∼0.8−0.9 $cm^2/(V\ s)$[23,25] and unprecedented stability.[27] In particular, the reported OFETs remained considerably more stable over time with exposure to oxygen, moisture, light, and heat as compared to similar pentacene-based devices.[23] PXX has also been used as a donor in charge-transfer complexes for n-channel organic field-effect transistors,[28] and its radical cation has been explored as a promising photo-oxidant.[29] Thus far, attempts at xylindein synthesis have proven incomplete.[30] The structure of xylindein was first reported in the 1960s[31,32] but its absolute configuration was unknown for many years, leading to a systematic re-examination in 2000 to obtain the xylindein tautomeric structure.[33] The developments utilizing derivatives with the PXX core[23,25,27−29] and our promising preliminary results incorporating xylindein in electronic devices[34,35] motivated the present paper, in which we investigate in detail the optical and (opto)electronic properties of naturally derived xylindein and xylindein-based films. In particular, we report on electron mobilities of up to 0.4 $cm^2/(V\ s)$ in amorphous pristine xylindein and xylindein:PMMA films, combined with high photo- and thermal stability of xylindein, and establish the mechanism of (photo)conduction in these films. We also reveal the presence of xylindein tautomers and aggregates and explore their contribution to optical and electronic properties of xylindein solutions and films. Finally, toward the development of sustainable naturally sourced electronic materials with enhanced processability, we investigate optical and (opto)-electronic properties of blends of xylindein with crystalline nanocellulose (CNC).

MATERIALS AND METHODS

Extraction of Xylindein. Over the past 5 years, we have developed a variety of protocols for cultivating fungi and extracting fungi-produced pigments.[36−38] Here, we focus on the wild-type xylindein, sustainably obtained from the decaying wood (Figure 1a,b), leaving a detailed comparison of characteristics of xylindein obtained via different preparation and purification protocols to a separate publication. Wild-type xylindein was harvested from wood (Figure 1a) collected at Tidewater, Oregon. Appropriate wood was identified by the signature blue-green color produced by *Chlorociboria* species, which is unique across several kingdoms. The *Chlorociboria* species responsible for staining the wood was identified as *C. aeruginosa* through DNA extraction and Sanger sequencing of the internal transcribed spacer region, followed by GenBank Megablast comparison (see the Supporting Information). The collected wood was crushed into approximately 2−3 mm fragments. The powder was placed in a 500 mL flask, with enough powder to cover the bottom of the flask in an even layer. Dichloromethane (DCM, 100 mL) was poured into the flask. The contents were then stirred on a magnetic stir plate for 1 h before being filtered, as described in ref 39. The solid crude xylindein was collected from the evaporated DCM solution, then sonicated in ethanol to form a suspension of xylindein aggregates. The ethanol solution was passed through a 0.45 μm poly(tetrafluoroethylene) filter, followed by multiple passes of clean ethanol through the filter to remove contaminants. The xylindein was removed from the filter with DCM, and solvents evaporated to yield solid xylindein powder.

Mass Spectrometry. The analysis was performed on a Shimadzu high-performance liquid chromatography (Colum-

DOI: 10.1021/acsomega.9b01490
ACS Omega 2019, 4, 13309−13318

bia, MD) coupled to a Waters Synapt HDRMS time-of-flight mass spectrometer (Milford, MA). The MS was operated in the positive ion mode, 80−1000 m/z scan range, 1 s scan time. A binary gradient and a 1.0 × 50 mm^2 Waters XBridge C18 column (Milford, MA) were used, for analytical separation. Solvent A consisted of MS grade water (Fisher Scientific, Fairlawn, NJ) and 0.1% formic acid (EMD Millipore Corporation, Billerica, MA). Solvent B consisted of MS grade acetonitrile (Fisher Scientific, Fairlawn, NJ) and 0.1% formic acid. High-resolution mass spectrometry of xylindein resulted in a measured mass of 569.1448 $(M + H)^+$, corresponding to the $(M + H)^+$ ion, $C_{32}H_{25}O_{10}$ (calculated exact mass of 569.1448, mass accuracy of 0.00 ppm), which is in agreement with the literature.[31,33]

Sample Preparation. For measurements of optical properties, xylindein powder was dissolved in various solvents (Figure 1c) including DCM, chloroform (CF), chlorobenzene (CB), tetrahydrofuran (THF), acetone (Ac), isopropyl alcohol, and water at various concentrations in the 10^{-6}−10^{-3} M range.

For the preparation of films, three types of solutions were prepared: xylindein dissolved in DCM at 10 mg/mL of the concentration, a mixture of 4 mg of xylindein with 1 mg of poly(methyl methacrylate) (PMMA) (Aldrich, M_w = 15 000) dissolved in 500 μL of DCM to form a 10 mg/mL solution, and a mixture of 4 mg of xylindein with 1 mg of crystalline nanocellulose (CNC) with 500 μL of formic acid to form a 10 mg/mL solution. CNC powder with fiber dimensions 5−20 nm wide by 150−200 nm long was obtained from the Process Development Center at the University of Maine.

For the film preparation, solutions of pristine xylindein or xylindein:PMMA or xylindein:CNC mixtures were drop-cast onto glass substrates patterned with Al or Au/Cr co-planar or interdigitated electrodes spaced by 25−200 μm.[40] The structure and morphology of drop-cast films was assessed using scanning electron microscopy (SEM) and X-ray diffraction (XRD), revealing the amorphous structure and morphology depending on the mixture, with blends yielding smoother films than pristine xylindein (Figure S1). The film thickness measured using a surface profilometer ranged between 3 and 5 μm, depending on the device.

Measurements. For optical absorption measurements in the solution and film, light from a halogen (LS-1, Ocean Optics) or Xe lamp (Oriel 96000) transmitted through samples was measured using an Ocean Optics USB2000 spectrometer. For photoluminescence (PL) measurements, the solution or film samples were excited with 633 nm light (HeNe laser). As the reference material for the PL quantum yield estimates, previously studied functionalized pentacene (Pn) derivative Pn-TIPS-F8 (also known as F8 TIPS-Pn) with QY = 0.6 in toluene was used.[41] PL emission was collected using an Ocean Optics USB2000-FLG spectrometer, as described in our previous publications.[42,43] Measurements of optical absorption and PL in films were conducted on an inverted microscope (Olympus IX-71) with a 10× objective in transmission and reflection geometry, respectively.

For measurements of photostability, 10 μM solutions of xylindein in chlorobenzene and of benchmark organic semiconductors, functionalized fluorinated anthradithiophene (ADT) derivative diF (triethylsilyl)ethynyl (TES)-ADT, and functionalized pentacene (triisopropylsilyl)ethynyl (TIPS)-Pn, in toluene were prepared,[41,42,44,45] and their optical absorption measured. The spectra were integrated in the S_0−S_1 absorption region (600−700 nm for xylindein, 450−550 nm for diF TES-ADT, and 560−660 nm for TIPS-Pn) yielding a data point at time t = 0. The solutions in vials sealed with a paraffin film to prevent solvent evaporation were then placed under the fume hood lights, in air, and the spectral measurement was repeated at various time intervals. The S_0−S_1 spectra were integrated and the result normalized by that at t = 0. The experiment was carried out up to 30 weeks.

For measurements of thermal stability, pristine xylindein films were placed on a hot plate held at a particular temperature in the 50−200 °C range for 2 h, in air. The absorption spectrum of the film was measured every 5 min. The spectra were integrated in the S_0−S_1 absorption region (600−750 nm) and plotted as a function of time, normalized at the value at t = 0.

For measurements of current−voltage characteristics, the voltage was applied to the samples using a Keithley 237 source measure unit, and current in the dark was measured as a function of applied voltage ranging from 0 to 300 V.

Continuous wave (cw) photocurrents in films were measured under 633 nm, 2 mW/cm^2 photoexcitation chopped using an optical chopper at 100 Hz. The voltage was applied to the samples using a Keithley 237 source measure unit, and the photocurrent was measured using a Stanford Research Systems (SRS830) lock-in amplifier.

For temperature-dependent measurements, samples were incorporated in an optical cryostat (Janis STC-500), and dark current and photocurrent measurements were carried out in the vacuum in the temperature range of 300−350 K.

Density Functional Theory (DFT) Calculations. The structure of xylindein was optimized using DFT methods in Gaussian 16 to ascertain the location and orientation of xylindein's hydroxyl groups. Initial structures of the molecule were optimized with the B3LYP function and 6-31G(d,p) basis set. Only configurations with centralized hydroxyl groups (Figure 1d) were found to be energetically stable, and of those, only two were found to have negligible dipole moments (Figure S2a,b), in keeping with our observations of enhanced solubility of xylindein in nonpolar, as compared to polar, solvents (discussed below). These two tautomers A and B were then optimized with a larger basis set (6-311G++(d,p)) to find the energies of the highest occupied molecular orbital (HOMO) and lowest unoccupied molecular orbital (LUMO). Time-dependent DFT methods were applied to find the energies of the vertical first allowed singlet excited state for xylindein embedded in the DCM solvent environment. A similar optimization process was conducted for dimethylxylindein (Figure S3), yielding only a single configuration. Properties of dimethylxylindein, embedded in a DCM solvent environment, were also calculated to assess the contribution of the OH groups, not present in dimethylxylindein, to various characteristics of xylindein. Control calculations were also conducted on several derivatives of peri-xanthenoxanthene (PXX) for comparisons with the literature, which are included in the Supporting Information.

Fit Procedure. The dilute solution absorption spectra of xylindein were initially fit using a vibronic progression model of eq 1[2,46−48]

$$\frac{A}{\hbar\omega} = A_0 \sum_{n=0}^{5} \frac{e^{-S} S^n}{n!} \Gamma_{\sigma_0(1+n\Delta\sigma)}(\hbar\omega - E_X - nE_V) \quad (1)$$

DOI: 10.1021/acsomega.9b01490
ACS Omega 2019, 4, 13309−13318

Here, $\frac{A}{\hbar\omega}$ represents the reduced absorption as a function of photon energy and A_0 is a scale factor for the integrated absorption of the exciton manifold. E_X is the 0−0 energy, E_V is the vibrational energy, n is an index for the number of vibrational quanta hosted by the molecule, and S is the corresponding Huang−Rhys factor. Each optical transition is modeled with a Lorentzian line shape Γ, with a full width at half maximum of σ_0 $(1 + n\Delta\sigma)$. Here, σ_0 is the 0−0 broadening, and $\Delta\sigma$ is the dimensionless progressive broadening factor, which corrects for vibrational modes not explicitly treated in the model.[47]

It was found that a single vibronic progression of eq 1 was insufficient to model the fine details in the xylindein spectra, so the spectra were then fit assuming the convolution of two vibronic progressions: $\frac{A_1}{\hbar\omega} + \frac{A_2}{\hbar\omega}$ (Figure 2b), each characterized by their own parameters E_X, E_V, S, σ_0, and $\Delta\sigma$ (Table 1).

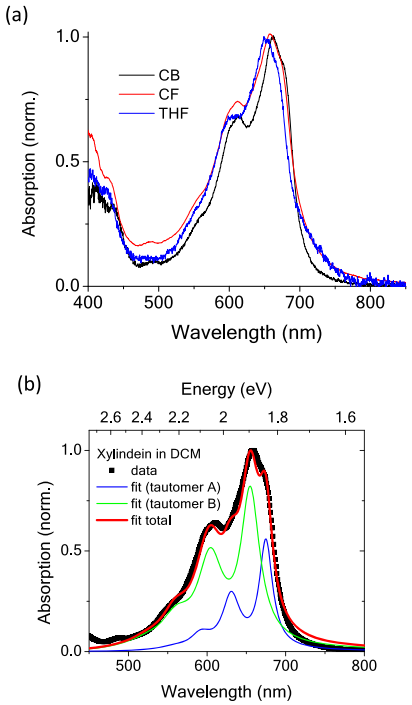

Figure 2. (a) Spectra of dilute solutions of xylindein in chlorobenzene (CB), chloroform (CF), and tetrahydrofuran (THF). (b) The absorption spectrum in DCM divided by $\hbar\omega$ and fit using two vibronic progressions, each described by eq 1. The fit parameters are listed in Table 1. The sum of the contributions of the two tautomers to the spectra is also included.

RESULTS AND DISCUSSION

Optical Properties. Optical absorption spectra of xylindein solutions in solvents of various polarities are shown in Figures 2 and S4. The most pronounced effect of the solvent polarity on xylindein spectra was in the solvent polarity-dependent propensity of xylindein for aggregation. At comparable concentrations, the contribution of xylindein aggregates to the spectra, which lead to the appearance of a new absorption band peaked at about ∼710−720 nm, was considerably higher as the solvent polarity increased. For example, in THF (dielectric constant ε = 7.9), the aggregate peak was pronounced at already 40 μM, whereas it was not present at 60 μM in CB (ε = 5.6), as shown in Figure S5a,b. For highly polar solvents, such as isopropyl alcohol (ε = 20), acetone (ε = 21), and water (ε = 80), even at micromolar concentrations, the aggregate peak was strongly pronounced (Figures 3a and S4). This is consistent with xylindein being a nonpolar molecule, and so its solubility in polar solvents is greatly reduced. The aggregates were also responsible for the near-infrared absorption spectra of xylindein-based films (Figure 3a) showing absorption features similar to those for xylindein in water.

Table 1. Fit Parameters Obtained from Fits of the Absorption Spectra to a Vibronic Progression of eq 1[a]

fit parameters	xylindein in CB (ε = 5.6)	xylindein in DCM (ε = 8.9)	dimethylxylindein in DCM
A_0 (norm)	0.35; 0.65	0.3; 0.7	1
E_X (eV)	1.82; 1.88	1.84; 1.90 [1.89; 1.93]	2.17 [2.14]
E_V (eV)	0.13; 0.16	0.13; 0.16	0.18
S	0.87; 0.87	0.77; 0.92	0.99
σ_0 (eV)	0.07; 0.09	0.06; 0.08	0.11
$\Delta\sigma$	0.51; 0.51	0.55; 0.59	0.53

[a]In the case of xylindein, a sum of two vibronic progressions, with the corresponding parameters listed, was needed to obtain a good fit. Numbers in the brackets correspond to values of vertical energies for two xylindein tautomers calculated as described in Materials and Methods.

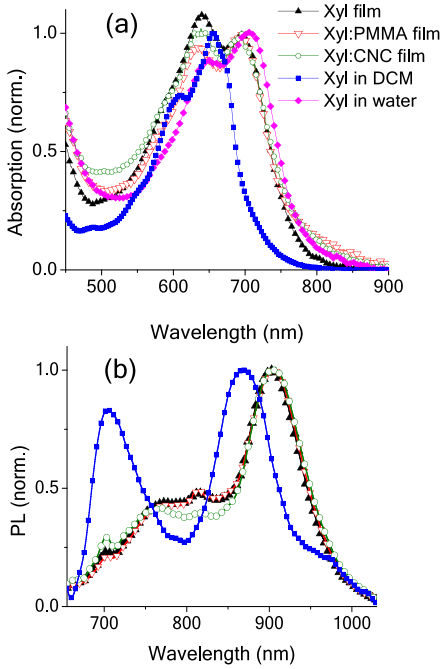

Figure 3. (a) Absorption spectra and (b) PL spectra obtained at 633 nm excitation of xylindein in solutions (e.g., in DCM and in water in (a) and in DCM in (b)), in pristine film, and in blends with PMMA and CNC. Symbols described in the legend of (a) also apply to (b). The PL spectra in (b) were not corrected for self-absorption.

To better understand the absorption spectra of xylindein, we fit the spectra as described in Materials and Methods. The parameters obtained from fits to the spectra of dilute solutions in CB and DCM are summarized in Table 1. The spectra of dilute solutions in these solvents exhibit a similar structure that can be fit by a sum of two vibronic progressions, each

DOI: 10.1021/acsomega.9b01490
ACS Omega 2019, 4, 13309−13318

described by eq 1 (Figure 2b). To understand the origin of the complicated structure of the S_0−S_1 spectrum of xylindein, we also modeled the absorption spectrum of the dimethylxylindein, in which the OH groups are substituted by the OMe groups (Figure S3b). The absorption spectrum of dimethylxylindein in DCM produced a good fit with one vibronic progression of eq 1, as shown in Figure S3a. Therefore, we attribute the need for two vibronic progressions to adequately describe the S_0−S_1 spectrum of xylindein to the presence of two tautomers, which exhibit slightly different energies for the 0−0 transition (E_X) and parameters describing the line shape and vibronic coupling in eq 1. Molecular structures of such tautomers were identified using DFT calculations as described in Materials and Methods and are shown in Figure S2a,b, with the relative contributions of tautomers A and B to the absorption spectra of about 30:70 (A_0 in Table 1). Their calculated vertical energies, which are comparable to the 0−0 energies (E_X) extracted from fits to the experimental data, are also included in Table 1.

In all xylindein solutions, the PL quantum yields measured at 633 nm excitation of the S_0−S_1 transition were below 0.1%. Such low quantum yields have been observed in other pigments such as indigo, for which it was attributed to the intramolecular proton transfer.[12,49] The mechanism of nonradiative energy relaxation in xylindein is currently under investigation and will be reported in our subsequent publication. The PL spectra obtained under 633 nm excitation of a DCM solution and of xylindein-based films are shown in Figure 3b. All films studied featured similar PL spectra, with a pronounced peak at ∼900 nm, which we attribute to xylindein aggregates. A similar peak was observed in concentrated solutions (e.g., at ∼870 nm, in addition to the xylindein monomer peak at ∼710 nm in Figure 3b), with the aggregate contribution increasing and exhibiting a red-shift with the xylindein concentration, due to changes in the dielectric environment.

Stability. Figure 4 illustrates a considerably higher photostability of xylindein in the solution as compared to

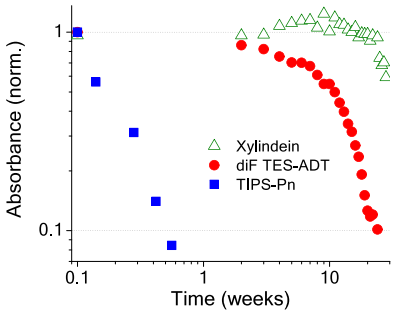

Figure 4. Integrated S_0−S_1 spectra, normalized at time t = 0, of dilute solutions of xylindein and of benchmark organic semiconductors TIPS-Pn and diF TES-ADT continuously exposed to light and air.

solutions of benchmark organic semiconductors TIPS-Pn and diF TES-ADT.[42,43] In particular, under continuous illumination in air, the TIPS-Pn molecules in the solution decomposed within 3 days. The fluorinated ADT derivative, diF TES-ADT, which has been photostable enough to enable its use as a fluorophore in single-molecule fluorescence spectroscopy,[41] showed a gradual degradation over the period of first several weeks followed by an accelerated degradation starting at about 5 weeks. Under the same conditions, no degradation in optical absorption of xylindein was observed over the period of about 25 weeks, after which some degradation occurred (Figure 4).

Enhanced photostability of pigments has been their known property for a long time, fostering their applications in art throughout the history[50,51] and more recently, as food colorants, paints,[52] and, finally, organic electronic devices.[8,13,53,54] The origin of high photostability depends on the molecular structure. For example, the photostability of indigo and its derivatives has been attributed to subpicosecond-excited intramolecular proton transfer leading to a rapid internal conversion.[12,49] This leads to short excited-state lifetimes, low PL quantum yields, and high photostability. Similar considerations could be operational in xylindein; ultrafast spectroscopy, which is necessary to quantify the picosecond time-scale excited-state dynamics and to reveal the contributing mechanism, is underway, and results will be reported elsewhere.

Xylindein also exhibited a relatively good thermal stability in air. For example, no considerable degradation of optical properties of xylindein films was observed upon holding the xylindein film at temperatures up to 100 °C in the air for at least 2 h (Figure S6). About 8 and 15% degradation occurred at 150 and 175 °C, respectively, after 2 h. At 200 °C, pronounced degradation occurred within the first 20 min of the heat treatment.

(Opto)electronic Properties. To better understand electronic properties of xylindein, we performed DFT calculations of the HOMO and LUMO orbitals for the tautomers A and B (Figure S2a,b, respectively) revealed by the combination of optical spectroscopy and DFT calculations. The HOMO and LUMO energies yielded −6.49 (−6.30) and −4.31 (−3.99) eV, respectively, for the tautomer A (B), resulting in the HOMO−LUMO gap of 2.19 (2.31) eV, as shown in Figure 5. The calculated HOMO and LUMO charge

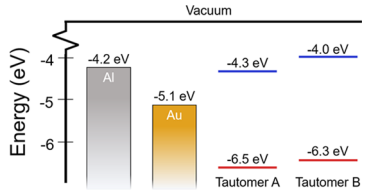

Figure 5. HOMO and LUMO energy levels for two xylindein tautomers. Work functions of Al and Au relative to the HOMO and LUMO energies are also shown.

densities for both tautomers are shown in Figure S2c−f. The low LUMO energies of xylindein suggest preferential electron or ambipolar transport, in contrast to the unsubstituted PXX, which favors hole transport.[24] Results from the cyclic voltammetry are consistent with this prediction, and the reversible reduction in xylindein was confirmed experimentally, as described in the Supporting information (Figure S7).

To explore electron transport in xylindein films, we prepared films on aluminum (Al) electrodes to facilitate electron injection expected from a relatively good alignment of Al work function with LUMO energies of xylindein (Figure 5). Figure 6 shows current−voltage (I−V) characteristics for two pristine xylindein films and for a xylindein:PMMA film, all on co-planar Al electrodes. The Ohmic response followed by a characteristic transition from the linear (I−V) to the space-charge-limited current (SCLC) (I−V^2) regime was observed in all samples. In the case of the planar electrode geometry used

DOI: 10.1021/acsomega.9b01490
ACS Omega 2019, 4, 13309−13318

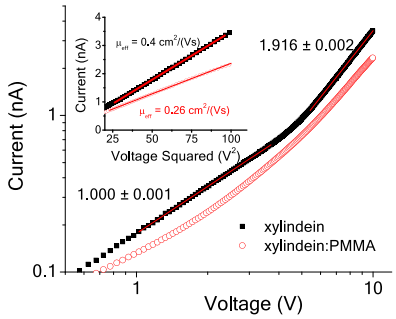

Figure 6. Current−voltage (I−V) characteristics for pristine xylindein and xylindein:PMMA films on co-planar Al electrodes with a 200 μm gap, showing the transition from the linear to the quadratic (SCLC) regime. The inset shows I vs V^2 and linear fits, slopes of which were used to calculate the effective mobilities assuming the thin-film approximation of the SCLCs in the planar electrode geometry, as discussed in the text.

in our experiments, the current flows along a thin layer of unknown thickness, and the current density (j) is expressed in units of A/m (as opposed to A/m^2 for the "sandwich" electrode geometry). Although there is no analytical solution for the relationship between the SCLC linear current density (j) and the applied voltage (V) in a film of finite thickness on co-planar electrodes, there are solutions for the extreme cases of the infinitely thin film ("thin-film approximation") and the infinite half-space ("infinite half-space approximation").[40] In the thin-film approximation, the linear current density[40] $j = (2/\pi)\mu_{\text{eff}}\varepsilon\varepsilon_0 V^2/L^2$. Here, $j = I/d$, where I is the measured current and d is the length of the electrode, L is the gap between the electrodes, ε_0 is the vacuum permittivity, ε is the dielectric constant (assumed here to be equal to 3), and μ_{eff} is the effective mobility. The SCLC j−V dependence in the infinite half-space approximation differs from the expression above only in the coefficient $2/\pi$, which is replaced by 0.28.[40] The thin-film approximation for our devices is justified by the $\lesssim$5 μm film thicknesses as compared to the gap between the electrodes (L) of 50−200 μm chosen for these experiments. From SCLC currents (the inset of Figure 6), values for the effective mobility in the 0.1−0.4 cm^2/(V s) range were obtained using the thin-film approximation, depending on the device, in pristine xylindein films. We consider these values to be lower bound estimates to the electron mobility, as the trap-free SCLC regime was not reached in our measurements and, thus, the intrinsic mobility is higher. We also note that the performance of xylindein-based devices depends on the fungi growth and purification protocols,[55] and higher mobilities could be possible with protocols other than the one used in the present study; this is currently under investigation. Achieving effective mobility values above 0.1 cm^2/(V s) is rather remarkable given that the films under study are amorphous, illustrating benefits of an interplay of intermolecular hydrogen bonding (Figure S8) and π−π stacking, afforded by the molecular structure of xylindein, for charge transport.

As xylindein tends to form porous and inhomogeneous films[34] (Figure S1a), to improve film processability, we also explored its blends with a polymer PMMA and a biopolymer CNC (both of which exhibited negligible electric currents in the absence of xylindein, thus providing a nonconductive scaffold for the xylindein molecules). The use of PMMA was inspired by our own[56] and other literature[57,58] studies of electronic properties of small-organic-semiconductor molecule:nonconductive polymer blends, which exhibited improved morphology and comparable or better electronic performance than that of pristine organic semiconductor films. The naturally sourced CNC was chosen to explore the possibility of creating the all-sustainable functional xylindein:polymer blend. Both blends yielded considerably smoother films (Figure S1b,c) as compared to xylindein films, with optical properties similar to those of pristine xylindein film (Figure 3), which suggests that the nature of xylindein aggregates is similar in all films. The xylindein:PMMA films yielded electric characteristics similar to those of the pristine xylindein films (Figures 6 and 7), with the

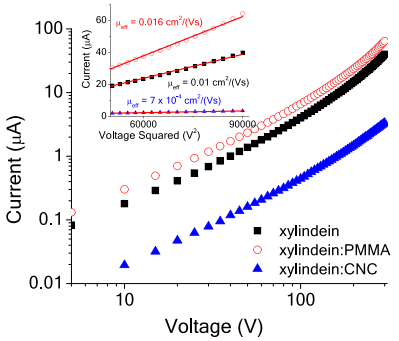

Figure 7. Current−voltage characteristics for pristine xylindein, xylindein:PMMA, and xylindein:CNC films on interdigitated Au electrodes with a 25 μm gap. The inset shows the high-voltage data for these three films replotted as a function of V^2, with linear fits that were used to calculate effective mobilities in the thin-film approximation of the SCLC in the planar electrode geometry, as discussed in the text.

SCLC effective mobilities similar to those in the pristine xylindein film (e.g., 0.26 cm^2/(V s) in the xylindein:PMMA film in Figure 6). The xylindein:CNC films exhibited electric currents and corresponding SCLC effective mobilities that were more than an order of magnitude lower than those in pristine xylindein or xylindein:PMMA blends, most likely due to a nonuniform distribution of xylindein in the CNC at high concentrations, which prevents the formation of the efficient conductive network via xylindein molecules.

In planar devices using gold (Au) electrodes, the transition from the linear to the quadratic SCLC regime was also observed in the current−voltage characteristics; however, it occurred at considerably higher voltages as compared to those in devices with Al electrodes, reflecting differences in the charge carrier injection properties depending on the electrode material. From the I vs V^2 linear fits to the SCLC regime in devices on planar Au electrodes (the inset of Figure 7), in the thin-film approximation, one obtains the effective mobilities μ_{eff} of ∼0.01, 0.016, and 7 × 10^{-4} cm^2/(V s) in pristine xylindein, xylindein:PMMA, and xylindein:CNC films, respectively. If the hole injection is dominant in these devices, the μ_{eff} values represent a lower bound on the hole mobility in these systems, as the trap-free regime was not achieved in these devices.[59] However, based on the alignment of the Au work function with the energy levels of xylindein (Figure 5), it is not clear whether the injection of a single type of the carrier can be ensured, in which case, the interpretation of the effective charge carrier mobility is considerably less straightforward[60] and it relies on the knowledge of recombination mobility, which is not known for our materials.

DOI: 10.1021/acsomega.9b01490
ACS Omega 2019, 4, 13309−13318

To probe the mechanism of conduction in xylindein-based films, we performed temperature-dependent measurements of electric currents in the dark and under a 633 nm cw photoexcitation. All samples exhibited a thermally activated response ($\sim\exp[-E_a/k_BT]$, where E_a is the activation energy, k_B is the Boltzmann constant, and T is the temperature) characterized by the activation energies E_a of 0.31, 0.25, and 0.24 eV for the dark currents in pristine xylindein, xylindein:PMMA, and xylindein:CNC films, respectively (Figure 8a). Such temperature dependence is, for example, characteristic of a hopping charge-transport mechanism in the exponentially distributed manifold of trap states with a characteristic energy E_a.[61] The obtained values of E_a are similar to those in a variety of amorphous polymers (e.g., E_a = 0.33 and 0.37 eV in polyfluorene-based derivatives poly(9,9′-dioctylfluorene-*co*-bis-*N*,*N*′-(4-butylphenyl)-bis-*N*,*N*′-phenyl-1,4-phenylene-diamine) and poly(9,9′-dioctylfluorene-*co*-benzothiadiazole), respectively) and organic glasses.[62−66] A reduction in the activation energy in blends as compared to pristine xylindein films is consistent with a more uniform morphology achieved in blends although one could argue that larger differences in the activation energies would be expected from the three types of samples with different morphologies used in our studies. It has been demonstrated that in organic semiconductor devices, the activation energy in charge carrier mobility measurements may have contributions from charge traps both from the bulk organic semiconductor material and from the interface with a substrate (formed by strain due to the mismatch in the thermal expansion coefficients between the organic semiconductor and the substrate). For example, the latter accounted for up to ∼0.1 eV differences in the activation energy observed in mobilities of P3HT transistors depending on the gate dielectric.[67] If the charge traps at the interface were responsible for most of the E_a in our samples, this would suggest that at the film−substrate interface, there is a thin xylindein layer with only a slightly different morphology in all three types of samples used in our studies. It is also interesting to note that the values of E_a are similar to the differences in the LUMO energy levels for the two xylindein tautomers, and so the presence of the two tautomers with offset energies, rather than the specific morphology of the films or of the interfacial layer, could dominate the disorder contributing to charge transport.

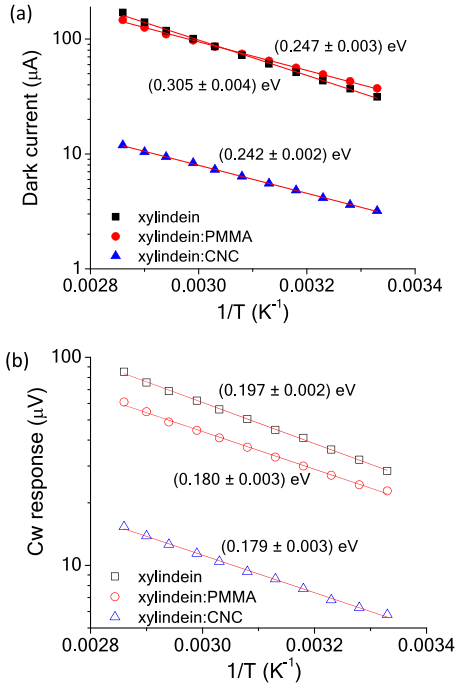

Figure 8. Temperature dependence of dark (a) and photo (b) currents obtained in pristine xylindein, xylindein:PMMA, and xylindein:CNC films on interdigitated Au electrodes with a 25 μm gap at 100 V. Arrhenius fits ($\sim\exp[-E_a/k_BT]$) with the extracted activation energies E_a are also included. The temperature dependence was independent of the applied voltage in the range studied.

All three types of xylindein-based films also exhibited photoresponse to a 633 nm continuous wave (cw) excitation.[34,35] The temperature dependence of the photocurrents revealed slightly lower activation energies as compared to dark currents (0.2 eV in pristine xylindein and 0.18 eV in xylindein-based blends), as shown in Figure 8b. These values are comparable to those obtained from photocurrents in various amorphous organic materials,[68−70] and the lower activation energies as compared to dark current activation energies have also been observed in organic glasses,[69] reflecting a slightly narrower energy manifold sampled by the photoexcited charge carriers as compared to injected carriers.

CONCLUSIONS

Optical and (opto)electronic properties of a naturally derived pigment xylindein and its blends with PMMA and CNC are presented. The analysis of the optical spectra revealed the presence of two tautomers whose structures and properties were explored using DFT. The propensity for xylindein aggregation depended on the solvent polarity and was strongly pronounced in polar solvents. Aggregates with similar optical properties were observed in films. Excellent photostability was observed in xylindein solutions as compared to those of benchmark organic semiconductor molecules. Electron mobility of up to 0.4 $cm^2/(V\ s)$ was obtained in amorphous films at room temperature. Both dark and photocurrent were thermally activated with activation energies of 0.3 and 0.2 eV, respectively, in pristine xylindein films. Xylindein blends with PMMA exhibited (opto)electronic performance comparable to that of pristine xylindein films. In xylindein blends with CNC, both dark and photocurrents were at least an order of magnitude lower than in pristine xylindein films. In both blends, the charge-transport activation energies were lower (0.25 eV) than in pristine xylindein films due to a smoother film morphology, as revealed by the SEM.

ASSOCIATED CONTENT

Supporting Information

The Supporting Information is available free of charge on the ACS Publications website at DOI: 10.1021/acsomega.9b01490.

SEM data, additional optical spectral data, thermal stability data, cyclic voltammetry data, FTIR data, and DFT calculations (PDF)

AUTHOR INFORMATION

Corresponding Author

*E-mail: oksana@science.oregonstate.edu (O.O.).

DOI: 10.1021/acsomega.9b01490
ACS Omega 2019, 4, 13309−13318

ORCID

Sarath M. Vega Gutierrez: 0000-0002-1882-8784
Oksana Ostroverkhova: 0000-0002-3833-161X

Funding

Funding through the National Science Foundation "Energy for Sustainability" program (CBET-1705099) is gratefully acknowledged.

Notes

The authors declare no competing financial interest.

■ ACKNOWLEDGMENTS

We thank Dr. I. Perez and Prof. D. Ji for the cyclic voltammetry measurements, Dr. G. Weber for the absorption spectrum of the dimethylxylindein, A. Fox and Prof. B. Gibbons for the XRD measurements, and T. Krueger and Prof. C. Fang for helpful discussions. Also acknowledged are J. Morré at the OSU Mass Spectrometry facility for assistance with mass spectrometry, J. Cappellazzi for help with fungal species identification, and P. Eschbach and T. Sawyer at OSU Electron Microscope Facility for assistance with SEM imaging. We also thank Prof. J. Anthony for TIPS-Pn, diF TES-ADT, and F8 TIPS-Pn.

■ ABBREVIATIONS

ADT, anthradithiophene; CB, chlorobenzene; CF, chloroform; CNC, crystalline nanocellulose; DCM, dichloromethane; DFT, density functional theory; HOMO, highest occupied molecular orbital; LUMO, lowest unoccupied molecular orbital; PMMA, poly(methyl methacrylate); PXX, peri-xanthenoxanthene; SCLC, space-charge-limited current; SEM, scanning electron microscopy; TES, (triethylsilyl)ethynyl; THF, tetrahydrofuran; TIPS, (triisopropylsilyl)ethynyl; XRD, X-ray diffraction

■ REFERENCES

(1) Ostroverkhova, O. *Handbook of Organic Materials for Electronic and Photonic Devices*, 2nd ed.; Elsevier, 2018.
(2) Ostroverkhova, O. Organic optoelectronic materials: mechanisms and applications. *Chem. Rev.* **2016**, *116*, 13279−13412.
(3) Arias, A. C.; MacKenzie, J. D.; McCulloch, I.; Rivnay, J.; Salleo, A. Materials and applications for large area electronics: solution-based approaches. *Chem. Rev.* **2010**, *110*, 3−24.
(4) Irimia-Vladu, M.; Sariciftci, N.; Bauer, S. Exotic materials for bio-organic electronics. *J. Mater. Chem.* **2011**, *21*, 1350−1361.
(5) Irimia-Vladu, M. "Green" electronics: biodegradable and biocompatible materials and devices for sustainable future. *Chem. Soc. Rev.* **2014**, *43*, 588−610.
(6) Głowacki, E. D.; Irimia-Vladu, M.; Bauer, S.; Sariciftci, N. S. Hydrogen-bonds in molecular solids − from biological systems to organic electronics. *J. Mater. Chem. B* **2013**, *1*, 3742.
(7) Głowacki, E. D.; Voss, G.; Leonat, L.; Irmia-Vladu, M.; Bauer, S.; Sariciftci, N. S. Indigo and Tyrian Purple−from ancient natural dyes to modern organic semiconductors. *Isr. J. Chem.* **2012**, *52*, 540−551.
(8) Irimia-Vladu, M.; Głowacki, E. D.; Troshin, P. A.; Schwabegger, G.; Leonat, L.; Susarova, D.; Krystal, O.; Ullah, M.; Kanbur, Y.; Bodea, M. A.; et al. Indigo-a natural pigment for high performance ambipolar organic field effect transistors and circuits. *Adv. Mater.* **2012**, *24*, 375−380.
(9) Guo, X.; Facchetti, A.; Marks, T. J. Imide- and amide-functionalized polymer semiconductors. *Chem. Rev.* **2014**, *114*, 8943−9021.
(10) Daniel Głowacki, E.; Leonat, L.; Irimia-Vladu, M.; Schwödiauer, R.; Ullah, M.; Sitter, H.; Bauer, S.; Sariciftci, N. Intermolecular hydrogen-bonded organic semiconductors-quinacridone versus pentacene. *Appl. Phys. Lett.* **2012**, *101*, No. 023305.
(11) Irimia-Vladu, M.; Sariciftci, N. S.; Bauer, S. Exotic materials for bio-organic electronics. *J. Mater. Chem.* **2011**, *21*, 1350−1361.
(12) Dittmann, M.; Graupner, F. F.; Maerz, B.; Oesterling, S.; Devivie-Riedle, R.; Zinth, W.; Engelhard, M.; Luettke, W. Photostability of 4,4′-dihydroxythioindigo, a mimetic of Indigo. *Angew. Chem., Int. Ed.* **2014**, *53*, 591−594.
(13) Głowacki, E. D.; Romanazzi, G.; Yumusak, C.; Coskun, H.; Monkowius, U.; Voss, G.; Burian, M.; Lechner, R. T.; Demitri, N.; Redhammer, G. J.; et al. Epindolidiones-versatile and stable hydrogen-bonded pigments for organic field-effect transistors and light-emitting diodes. *Adv. Funct. Mater.* **2015**, *25*, 776−787.
(14) Robinson, S. C. Developing fungal pigments for "painting" vascular plants. *Appl. Microbiol. Biotechnol.* **2012**, *93*, 1389−1394.
(15) Blanchette, R. A.; Wilmering, A. M.; Baumeister, M. The use of green-stained wood caused by the fungus *Chlorociboria* in intarsia masterpieces from the 15th century. *Holzforschung* **1992**, *46*, 225−232.
(16) Robinson, S. C.; Michaelsen, H.; Robinson, J. *Spalted Wood. The History, Science, and Art of a Unique Material*; Schiffer Publishing, 2016.
(17) Weber, G. L.; Boonloed, A.; Naas, K. M.; Koesdojo, M. T.; Remcho, V. T.; Robinson, S. C. A Method to stimulate production of extracellular pigments from wood-degrading fungi using a water carrier. *Curr. Res. Environ. Appl. Mycol.* **2016**, *6*, 218−230.
(18) Robinson, S. C.; Hinsch, E.; Weber, G.; Freitas, S. Method of extraction and resolubilisation of pigments from *Chlorociboria aeruginosa* and *Scytalidium cuboideum*, two prolific spalting fungi. *Color. Technol.* **2014**, *130*, 221−225.
(19) Robinson, S. C.; Tudor, D.; Snider, H.; Cooper, P. A. Stimulating growth and xylindein production of *Chlorociboria aeruginascens* in agar-based systems. *AMB Express* **2012**, *2*, 15.
(20) Robinson, S. C.; Hinsch, E.; Weber, G.; Leipus, K.; Cerney, D. Wood colorization through pressure treating: the potential of extracted colorants from spalting fungi as a replacement for woodworkers' aniline dyes. *Materials* **2014**, *7*, 5427−5437.
(21) Robinson, S. C.; Laks, P. E. Wood species affects laboratory colonization rates of *Chlorociboria* Sp. *Int. Biodeterior. Biodegrad.* **2010**, *64*, 305−308.
(22) Song, C.; Swager, T. M. Conducting polymers containing peri -xanthenoxanthenes via oxidative cyclization of binaphthols. *Macromolecules* **2009**, *42*, 1472−1475.
(23) Kobayashi, N.; Sasaki, M.; Nomoto, K. Stable peri-xanthenoxanthene thin-film transistors with efficient carrier injection. *Chem. Mater.* **2009**, *21*, 552−556.
(24) Wang, L.; Duan, G.; Ji, Y.; Zhang, H. Electronic and charge transport properties of peri-xanthenoxanthene: the effects of heteroatoms and phenyl substitutions. *J. Phys. Chem. C* **2012**, *116*, 22679−22686.
(25) Mei, J.; Diao, Y.; Appleton, A. L.; Fang, L.; Bao, Z. Integrated materials design of organic semiconductors for field-effect transistors. *J. Am. Chem. Soc.* **2013**, *135*, 6724−6746.
(26) Lv, N.; Xie, M.; Gu, W.; Ruan, H.; Qiu, S.; et al. Synthesis, properties, and structures of functionalized peri -xanthenoxanthene. *Org. Lett.* **2013**, *15*, 2382−2385.
(27) Yoneya, N.; Ono, H.; Ishii, Y.; Himori, K.; Hirai, N.; Abe, H.; Yumoto, A.; Kobayashi, N.; Nomoto, K. Flexible electrophoretic display driven by solution-processed organic thin-film transistors. *J. Soc. Inf. Disp.* **2012**, *20*, 143−147.
(28) Yokokura, S.; Takahashi, Y.; Hasegawa, H.; Harada, J.; Inabe, T.; Matsushita, M. M.; Awaga, K. Transport characteristics of the organic field-effect transistors based on charge transfer complex as semiconductors. *J. Nanosci. Nanotechnol.* **2016**, *16*, 3355−3359.
(29) Christensen, J. A.; Zhang, J.; Zhou, J.; Nelson, J. N.; Wasielewski, M. R. Near-infrared excitation of the peri-xanthenoxanthene radical cation drives energy-demanding hole transfer reactions. *J. Phys. Chem. C* **2018**, *122*, 23364−23370.
(30) Donner, C. D.; Cuzzupe, A. N.; Falzon, C. L.; Gill, M. Investigations towards the synthesis of xylindein, a blue-green

DOI: 10.1021/acsomega.9b01490
ACS Omega 2019, 4, 13309−13318

pigment from the fungus *Chlorociboria aeruginosa*. *Tetrahedron* **2012**, *68*, 2799−2805.
(31) Edwards, R. L.; Kale, N. The structure of xylindein. *Tetrahedron* **1965**, *21*, 2095−2107.
(32) Blackburn, G. M.; Neilson, A.; Todd, A. Structure of xylindein. *Proc. Chem. Soc., London* **1962**, 327−328.
(33) Saikawa, Y.; Watanabe, T.; Hashimoto, K.; Nakata, M. Absolute configuration and tautomeric structure of xylindein, a blue-green pigment of *Chlorocibor*ia species. *Phytochemistry* **2000**, *55*, 237−240.
(34) Giesbers, G.; Van Schenck, J.; Gutierrez, S. V.; Robinson, S.; Ostroverkhova, O. Fungi-derived pigments for sustainable organic (opto)electronics. *MRS Adv.* **2018**, *3*, 3459−3464.
(35) Harrison, R.; Quinn, A.; Weber, G.; Johnson, B.; Rath, J.; Remcho, V.; Robinson, S.; Ostroverkhova, O. Fungi-derived pigments as sustainable organic (opto)electronic materials. *Proc. SPIE* **2017**, *10101*, No. 101010U.
(36) Weber, G.; Boonloed, A.; Naas, K. M.; Koesdjojo, M. T.; Remcho, V. T.; Robinson, S. C. A method to stimulate production of extracellular pigments from wood- degrading fungi using a water carrier. *Curr. Res. Environ. Appl. Mycol.* **2016**, *6*, 218−230.
(37) Weber, G.; Chen, H. L.; Hinsch, E.; Freitas, S.; Robinson, S. Pigments extracted from the wood-staining fungi *Chlorociboria aeruginosa*, *Scytalidium cuboideum*, and *S. ganodermophthorum* show potential for use as textile dyes. *Color. Technol.* **2014**, *130*, 445−452.
(38) Boonloed, A.; Weber, G. L.; Ramzy, K. M.; Dias, V. R.; Remcho, V. T. Centrifugal partition chromatography: a preparative tool for isolation and purification of xylindein from *Chlorociboria aeruginosa*. *J. Chromatogr. A* **2016**, *1478*, 19−25.
(39) Robinson, S. C.; Gutierrez, V. S.; Cespedes, R. A.; Iroume, N.; Vorland, N. R.; McClelland, A.; Huber, M.; Stanton, S. Potential for carrying pigments derived from spalting fungi in natural oils. *J. Coat. Technol. Res.* **2017**, *14*, 1107−1113.
(40) Day, J.; Platt, A. D.; Subramanian, S.; Anthony, J. E.; Ostroverkhova, O. Influence of organic semiconductor-metal interfaces on the photoresponse of functionalized anthradithiophene thin films. *J. Appl. Phys.* **2009**, *105*, No. 103703.
(41) Shepherd, W. E. B.; Grollman, R.; Robertson, A.; Paudel, K.; Hallani, R.; Loth, M. A.; Anthony, J. E.; Ostroverkhova, O. Single-molecule imaging of organic semiconductors: toward nanoscale insights into photophysics and molecular packing. *Chem. Phys. Lett.* **2015**, *629*, 29−35.
(42) Platt, A. D.; Day, J.; Subramanian, S.; Anthony, J. E.; Ostroverkhova, O. Optical, fluorescent, and (photo)conductive properties of high-performance functionalized pentacene and anthradithiophene derivatives. *J. Phys. Chem. C* **2009**, *113*, 14006−14014.
(43) Platt, A. D.; Kendrick, M. J.; Loth, M.; Anthony, J. E.; Ostroverkhova, O. Temperature dependence of exciton and charge carrier dynamics in organic thin films. *Phys. Rev. B* **2011**, *84*, No. 235209.
(44) Paudel, K.; Johnson, B.; Thieme, M.; Haley, M. M.; Payne, M. M.; Anthony, J. E.; Ostroverkhova, O. Enhanced charge photogeneration promoted by crystallinity in small-molecule donor-acceptor bulk heterojunctions. *Appl. Phys. Lett.* **2014**, *105*, No. 043301.
(45) Day, J.; Platt, A. D.; Ostroverkhova, O.; Subramanian, S.; Anthony, J. E. Organic semiconductor composites: influence of additives on the transient photocurrent. *Appl. Phys. Lett.* **2009**, *94*, No. 013306.
(46) Van Schenck, J. D. B.; Giesbers, G.; Kannegulla, A.; Cheng, L.; John, E.; Ostroverkhova, O. Molecular packing-dependent exciton and polariton dynamics in anthradithiophene organic crystals. *MRS Adv.* **2018**, *3*, 3465−3470.
(47) Yamagata, H.; Maxwell, D. S.; Fan, J.; Kittilstved, K. R.; Briseno, A.; Barnes, M. D.; Spano, F. C. HJ-aggregate behaviour of crystalline 7,8,15,16-tetraazaterrylene: introducing a new design paradigm for organic materials. *J. Phys. Chem. C* **2014**, *118*, 28842−28854.
(48) Hestand, N. J.; Spano, F. C. Expanded theory of H- and J -molecular aggregates: the effects of vibronic coupling and intermolecular charge transfer. *Chem. Rev.* **2018**, *118*, 7069−7163.
(49) Yamazaki, S.; Sobolewski, A.; Domcke, W. Molecular mechanisms of the photostability of Indigo. *Phys. Chem. Chem. Phys.* **2011**, *13*, 1618−1628.
(50) Robinson, S. The Fine Art of Decay. *Am. Sci.* **2014**, *102*, 206−213.
(51) Miliani, C.; Monico, L.; Melo, M. J.; Fantacci, S.; Angelin, E. M.; Romani, A.; Janssens, K. Photochemistry of artists dyes and pigments: towards better understanding and prevention of colour change in works of art. *Angew. Chem., Int. Ed.* **2018**, *57*, 7324−7334.
(52) Hinsch, E.; Robinson, S. Fungal Pigments as Textlile Dyes. In *Handbook of Textile Coloration and Finishing*; Shahid, M., Tang, R., Chen, G., Eds.; Studium Press, 2016.
(53) Chen, T. L.; Chen, J. J. A.; Catane, L.; Ma, B. Fully solution processed p-i-n organic Solar cells with an industrial pigment - quinacridone. *Org. Electron.* **2011**, *12*, 1126−1131.
(54) Nielsen, C. B.; Turbiez, M.; McCulloch, I. Recent advances in the development of semiconducting DPP-containing polymers for transistor applications. *Adv. Mater.* **2013**, *25*, 1859−1880.
(55) Giesbers, G.; Krueger, T.; Van Schenck, J.; Van Court, R.; Morre, J.; Fang, C.; Robinson, S.; Ostroverkhova, O. Fungi-derived xylindein: effect of purity on optical and electronic properties. *MRS Adv.* **2019**, 1.
(56) Shepherd, W. E. B.; Platt, A. D.; Hofer, D.; Ostroverkhova, O.; Loth, M.; Anthony, J. E. Aggregate formation and its effect on (opto)electronic properties of guest-host organic semiconductors. *Appl. Phys. Lett.* **2010**, *97*, No. 163303.
(57) Smith, J.; Zhang, W.; Sougrat, R.; Zhao, K.; Li, R.; Cha, D.; Amassian, A.; Heeney, M.; McCulloch, I.; Anthopoulos, T. D. Solution-processed small molecule-polymer blend organic thin-film transistors with hole mobility greater than 5 cm^2/Vs. *Adv. Mater.* **2012**, *24*, 2441−2446.
(58) Niazi, M. R.; Li, R.; Li, E. Q.; Kirmani, A. R.; Abdelsamie, M.; Wang, Q.; Pan, W.; Payne, M. M.; Anthony, J. E.; Smilgies, D.-M.; et al. Solution-printed organic semiconductor blends exhibiting transport properties on par with single crystals. *Nat. Commun.* **2015**, *6*, No. 8598.
(59) Blakesley, J. C.; Castro, F. A.; Kylberg, W.; Dibb, G. F. A.; Arantes, C.; Valaski, R.; Cremona, M.; Soo, J.; Kim, J. Towards reliable charge-mobility benchmark measurements for organic semiconductors. *Org. Electron.* **2014**, *15*, 1263−1272.
(60) Goetz, K.; Jurchescu, O. Conductivity Measurements of Organic Materials Using Field-Effect Transistors (FETs) and Space-Charge-Limited Current (SCLC) Techniques. In *Handbook of Organic Materials for Electronic and Photonic Devices*; Ostroverkhova, O., Ed.; Woodhead Publishing, 2018; pp 453−488.
(61) Baranovskii, S. D. Theoretical description of charge transport in disordered organic semiconductors. *Phys. Status Solidi B* **2014**, *251*, 487−525.
(62) Hou, Z.; You, W.; Yu, L. Effect of a trapping molecule on the monolithic organic photorefractive materials. *Appl. Phys. Lett.* **2004**, *85*, 5221−5223.
(63) Martin, S. J.; Lupton, J. M.; Samuel, I. D. W.; Walker, A. B. Modelling temperature-dependent current voltage characteristics of an MEH-PPV organic light emitting device. *J. Phys.: Condens. Matter* **2002**, *14*, 9925−9933.
(64) Blakesley, J. C.; Clubb, H. S.; Greenham, N. C. Temperature-dependent electron and hole transport in disordered semiconducting polymers: analysis of energetic disorder. *Phys. Rev. B* **2010**, *81*, No. 045210.
(65) Blom, P. W. M.; Vissenberg, M. C. J. M. Charge transport in poly (p-phenylene vinylene) light-emitting diodes. *Mater. Sci. Eng., R* **2000**, *27*, 53−94.
(66) Choudhury, K. R.; Samoc, M.; Patra, A.; Prasad, P. N. Charge carrier transport in poly(N -vinylcarbazole): CdS Quantum Dot Hybrid Nanocomposite. *J. Phys. Chem. B* **2004**, *108*, 1556−1562.

DOI: 10.1021/acsomega.9b01490
ACS Omega 2019, 4, 13309−13318

(67) Mei, Y.; Diemer, P.; Niazi, M.; Hallani, R.; Jarolimek, K.; Day, C.; Risko, C.; Anthony, J.; Amassian, A.; Jurchescu, O. Crossover from band-like to thermally activated charge transport in organic transistors due to strain-induced traps. *Proc. Natl. Acad. Sci. U.S.A.* **2017**, *114*, E6739−E6748.
(68) Kishore, V. C.; Dhanya, R.; Kartha, C. S.; Sreekumar, K.; Joseph, R. Photoconductivity in molecularly doped poly-(methylmethacrylate) sandwich cells. *J. Appl. Phys.* **2007**, *101*, No. 063102.
(69) Ostroverkhova, O.; He, M.; Twieg, R. J.; Moerner, W. E. Role of temperature in controlling performance of photorefractive organic glasses. *ChemPhysChem* **2003**, *4*, 732−744.
(70) Day, J.; Subramanian, S.; Anthony, J. E.; Lu, Z.; Twieg, R. J.; Ostroverkhova, O. Photoconductivity in organic thin films: from picoseconds to seconds after excitation. *J. Appl. Phys.* **2008**, *103*, No. 123715.

DOI: 10.1021/acsomega.9b01490
ACS Omega 2019, 4, 13309−13318